ATMOSPHERIC
ENVIRONMENT
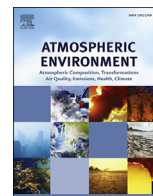
Carbonaceous aerosols in megacity Xi'an, China: Implications of thermal/optical protocols comparison

Y.M. Han [a, b, *], L.-W.A. Chen [c, d], R.-J. Huang [a, e], J.C. Chow [a, d], J.G. Watson [a, d], H.Y. Ni [a],
S.X. Liu [a], K.K. Fung [f], Z.X. Shen [b], C. Wei [a, g], Q.Y. Wang [a], J. Tian [a], Z.Z. Zhao [a],
André S.H. Prévôt [a, e], J.J. Cao [a]

[a] SKLLQG and Key Lab of Aerosol Chemistry & Physics, Institute of Earth Environment, Chinese Academy of Sciences, Xi'an, 710061, China
[b] School of Human Settlements and Civil Engineering, Xi'an Jiaotong University, Xi'an, 710049, China
[c] Department of Environmental and Occupational Health, University of Nevada, Las Vegas, NV, 89154, USA
[d] Division of Atmospheric Sciences, Desert Research Institute, 2215 Raggio Parkway, Reno, NV, 89512, USA
[e] Laboratory of Atmospheric Chemistry, Paul Scherrer Institute (PSI), 5232, Villigen, Switzerland
[f] AtmAA Inc., 23917 Craftsman Road, Calabasas, CA, 91302, USA
[g] SCDRC, Shanghai Advanced Research Institute, Chinese Academy of Sciences, Shanghai 201210, China

HIGHLIGHTS

- OC/EC split ratio is a key to evaluate the cooling versus warming effects of aerosols.
- Over twofold difference in EC concentrations and OC/EC ratios by different protocols.
- Good correlations between char and HULIS-C suggest common sources, likely the widespread biomass burning in the region.
- Char/soot ratios contrast OC/EC ratios in seasonal variation.
- Char and soot should be considered in chemical transport and climate models.

GRAPHICAL ABSTRACT
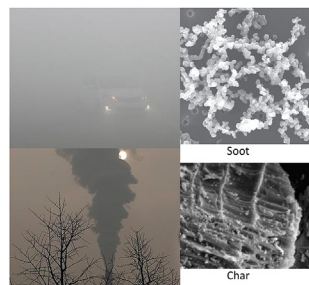
ARTICLE INFO

ABSTRACT

Carbonaceous aerosol is an important component that influences the environment, climate, and human health. Organic and elemental carbon (OC and EC) are the two main constituents of carbonaceous aerosols that have opposite, i.e., cooling versus warming, effects on the Earth's radiation balance. Knowledge on the variability of OC/EC splits measured by different thermal/optical protocols is useful for understanding the uncertainty in the climate models. This study shows good correlations within OC or EC ($r^2 > 0.83$, P < 0.001) across the IMPROVE, IMPROVE_A, and EUSAAR_2 protocols for both ambient aerosol samples and biomass burning samples. However, EC concentrations differ by more than two folds, and OC/EC ratios differ up to a factor of 2.7. The discrepancies were attributed to the selection between the reflectance and transmittance corrections and the different peak inert-atmosphere temperature. The IMPROVE and IMPROVE_A protocols also quantified different char and soot concentrations, two subtypes of EC with distinct chemical and optical properties. Char, but not soot, was found to correlate with the humic-like substances (HULIS) content in the samples, suggesting that both char and

* Corresponding author. 97 Yanxiang Road, Yanta Zone, Xi'an, 710061, China.
  E-mail address: yongming@ieecas.cn (Y.M. Han).

Biomass burning emissions
Temporal variations
Climatic implications

HULIS originate mainly from biomass burning. A one-year (2012–2013) ambient aerosol monitoring in Xi'an, China, shows that OC, EC, and char displayed winter highs and summer lows, while soot had no seasonal trend. The char/soot ratios showed a "single peak" in winter, while OC/EC ratios exhibited "dual peak" feature due to the influence of secondary organic aerosol formation. In addition to commonly measured OC and EC, we recommend both char and soot from a common reference method to be considered in the chemical transport and climate models.

1. Introduction

Carbonaceous aerosol constitutes 20–50% of $PM_{2.5}$ mass (particulate matter with an aerodynamic diameter $\leq$2.5 μm) in most urban areas (Cao et al., 2007; Huang et al., 2014) and is influencing Earth's climate directly by absorbing and scattering radiation and indirectly by acting as cloud condensation and ice nuclei for cloud and precipitation formation (Jacobson, 2001; Ramanathan and Carmichael, 2008). Carbonaceous aerosol also adversely affects visibility (Watson, 2002) and human health (Janssen et al., 2012; Mauderly and Chow, 2008). However, uncertainties exist due to the complexity of carbonaceous aerosol. Atmospheric carbonaceous aerosol is commonly classified into organic carbon (OC) and elemental carbon (EC). EC, also known as black carbon (BC), is the most important light-absorbing aerosol component in the atmosphere, with an estimated climate forcing of +0.88 (range +0.17–+1.48) W m^{-2} (Bond et al., 2013), ranked as the second largest contributor to anthropogenic radiative forcing after carbon dioxide (CO_2). On the contrary, OC can cool the atmosphere by increasing the Earth's reflectivity (Chameides and Bergin, 2002). OC and inorganic composition of aerosol can also influence the absorption of EC through lensing effect (Wang et al., 2014). The net climate forcing of carbonaceous aerosol is strongly determined by the OC/EC ratio (Novakov et al., 2005; Saleh et al., 2014; Sato et al., 2003).

OC and EC are operationally defined and there is no universally accepted standard method for quantification. The most widely used is the thermal/optical (TO) method (Watson et al., 2005), which has been practiced for over three decades (Gray et al., 1984). Different protocols have been applied (Birch and Cary, 1996; Cavalli et al., 2010; Chow et al., 1993), and comparisons between the different protocols have been made (Chow et al., 2001; Hitzenberger et al., 2006; Hitzenberger and Tohno, 2001; Reisinger et al., 2008). Watson et al. (2005) summarized that while being able to measure total carbon (TC), sum of OC and EC, consistently in aerosol samples, different TO protocols reported large discrepancy (up to a factor of 7) in EC concentrations.

The IMPROVE (Interagency Monitoring of Protected Visual Environments) and IMPROVE_A protocols (Chow et al., 2007) have been implemented in the U.S. Environmental Protection Agency (EPA) non-urban IMPROVE Network and urban Chemical Speciation Network (CSN) since 1987/88 and 2006/07 respectively. Over 200,000 p.m. samples worldwide have been analyzed. The transition of IMPROVE protocol by DRI/OGC analyzer to IMPROVE_A protocol by DRI model 2001 analyzer (Atmoslytic Inc., Calabasas, CA, USA) occurred around 2005. The two protocols differ in temperature by 20–40 °C at each temperature plateau (Table 1) due to the difference between filter and thermocouple temperatures in DRI/OGC analyzer (Chow et al., 2005).

Over the past decade both IMPROVE and IMPROVE_A protocols have been implemented in China using the DRI Model 2001 analyzer e.g. (Cao et al., 2003, 2013; Han et al., 2010), but without

distinguishing the difference of the two protocols. Chow et al. (2004) show that IMPROVE reflectance pyrolysis adjustment (i.e., thermal/optical reflectance [TOR]) yielded similar EC results regardless of the temperature protocol used for samples in the U.S.A. However, quantitative comparisons between the two protocols have not been examined in China, especially in urban areas with abundant biomass burning contributions (Huang et al., 2014; Zhang et al., 2014).

The EUSAAR_2 (European Supersites for Atmospheric Aerosol Research) protocol (Cavalli et al., 2010) has been widely used in Europe. This protocol is a modification of the National Institute of Occupational Safety and Health (NIOSH)-like thermal/optical transmission (TOT) protocol with fixed heating duration (Table 1). How it performs for Chinese aerosol samples, with their concentrations being often one order magnitude higher than European samples, needs a further investigation and comparison with IMPROVE and IMPROVE_A protocols.

Han et al. (2007) divided EC into two subtypes: char and soot, corresponding to EC evolved at low temperatures (i.e., 550 or 580 °C in oxidizing atmosphere) representing combustion residues by pyrolysis in smoldering fires, and EC evolved in high temperatures (i.e., >700 or 740 °C in oxidizing atmosphere) representing refractory condensation formed from volatiles in high-temperature flaming fires, respectively (Han et al., 2010; Janssen et al., 2012). Char and soot have different physico-chemical characteristics (Goldberg, 1985; Hammes et al., 2007; Han et al., 2010; Masiello, 2004), with soot being more light absorbing than char (Han et al., 2010). Another light-absorbing component is brown carbon (BrC), an OC component that could originate from smoldering biomass burning or secondary organic aerosol (Andreae and Gelencser, 2006). The chemical nature of BrC is not well elucidated, and it is believed to contain polycyclic aromatic hydrocarbons (PAHs), branched, oxygenated, and/or nitro-PAHs, as well as polycarboxylic acid or humic-like substances (HULIS) (Graber and Rudich, 2006;

Table 1
Temperature (°C) and time (s) protocols for the three thermal optical methods (IMPROVE, IMPROVE_A, and EUSAAR_2) used in this study.

Step	Gas	IMPROVE		IMPROVE_A		EUSAAR_2	
		Temp	Time[a]	Temp	Time[a]	Temp	Time[b]
OC1	pure He	120	150–580	140	150–580	200	120
OC2	pure He	250	150–580	280	150–580	300	150
OC3	pure He	450	150–580	480	150–580	450	180
OC4	pure He	550	150–580	580	150–580	650	180
EC1	2%O_2/98%He	550	150–580	580	150–580	500	120
EC2	2%O_2/98%He	700	150–580	740	150–580	550	120
EC3	2%O_2/98%He	800	150–580	840	150–580	700	70
EC4	2%O_2/98%He	n/a	n/a	n/a	n/a	850	80
Detector		Methanator/FID					
Pyrolysis correction		Reflectance & transmittance					

[a] time duration is flexible
[b] time duration is constant.

Hoffer et al., 2006). Several studies have reported substantial HULIS production from biomass burning, particularly the smoldering phase (Asa-Awuku et al., 2008; Hoffer et al., 2006; Lin et al., 2010a; Mayol-Bracero et al., 2002).

As part of an effort to reconcile measurements made by different carbon analyzing protocols in China, this study aimed to evaluate OC and EC measurements as well as char/soot separation in Chinese urban aerosol samples by IMPROVE, IMPROVE_A and EUSAAR_2 protocols using the DRI Model 2001 analyzer. Ambient $PM_{2.5}$ samples from Xi'an, China and source samples from biomass burning were studied. Seasonal variations in TC, OC, EC, char, and soot are discussed in light of potential $PM_{2.5}$ sources and climatic impacts. In addition, the correlations of HULIS with char and soot measured by IMPROVE and IMPROVE_A were investigated to better understand the source of HULIS.

2. Experimental

2.1. Ambient samples

Xi'an city (33°29′−34 44′ N, 107 40′−109 49′ E) located in the Guanzhong Basin is one of the largest tourist cities and on the list of the ten most polluted cities in China (CNEMC, 2013). Biomass burning during winter contributes to >50% of the TC (Zhang et al., 2014). $PM_{2.5}$ samples were collected from the rooftop of a building ~20 m above ground in the campus of Xi'an Jiaotong University using a mini-volume sampler (Airmetrics, Springfield, OR, USA) operating at a flow rate of 5 L min^{-1}. Sampling was conducted over a 24-h period (10:00 a.m. to 10:00 a.m. the next day) every 6 days from March 10, 2012 to March 11, 2013. All samples were collected on pre-fired (850 °C for 3 h) and pre-weighed 47 mm Whatman quartz-fiber filters and then stored in a freezer (−20 °C) until analysis.

2.2. Biomass combustion samples

Agricultural waste including wheat straw, rice straw, and corn stalk were collected from the main producing areas in China. Combustion experiments were conducted in a combustion chamber at the Institute of Earth Environment, Chinese Academy of Sciences (IEECAS). The combustion chamber (Tian et al., 2015) has a total volume of ~8 m^3 equipped with a thermocouple, a thermoanemometer, a custom-built purified air inlet, and a dilution system for sampling. The fuels were burned on a platform inside the combustion chamber, and $PM_{2.5}$ were sampled by the dilution sampler through three parallel sampling channels (i.e., one Teflon and two quartz-fiber filters) at a sampling flow rate of 5 L min^{-1} for each channel. Samples from 20 combustion experiments were acquired.

2.3. Carbon analysis

Mass concentrations were gravimetrically measured using an electronic microbalance with ±1 μg sensitivity (Sartorius, Gottingen, Germany), after which a 0.526 cm^2 punch of the filter was taken for carbon analyses. Each of these TO protocols contains two stages: the first is in an inert atmosphere where OC fractions (i.e., OC1-4, see Table 1) are evolved, with the assumption that low-volatility EC fractions are not liberated in an inert helium (He) atmosphere; and the second is in an oxidation atmosphere (98%He/2%O_2) that evolves the EC fractions (i.e., EC1-4, see Table 1). An oxidizer (manganese dioxide [MnO_2] at 800−900 °C) converts the liberated carbon compounds to CO_2, which is then reduced to methane (CH_4) by a methanator and quantified by a flame ionization detector (FID). Heating in an inert environment can generate

some pyrolyzed organic carbon (POC), and a laser (633 nm) is used to monitor the reflectance and transmittance of a filter during thermal analysis. POC is defined as the carbon measured after the introduction of a He/O_2 atmosphere, but before a split point where reflectance (POC_R) or transmittance (POC_T) returned to its initial value, while OC and EC are defined as carbon measured before and after the optical split point, respectively. This adjustment assumes that POC attenuates the laser in a similar way as the native EC, although this may not be always true (Chen et al., 2004). TOR and TOT are referred to the reflectance and transmittance pyrolysis adjustment, respectively.

Alternatively, POC may be estimated from the incremental light attenuation throughout the inert heating stage ($\tau_{ATN,POC}$), thus

$$\tau_{ATN,POC} = -\ln\left(\frac{T_{min}}{T_0}\right) \tag{1}$$

where T_0 and T_{min} are initial and minimum transmittance, measured at the beginning and end of the inert heating stage, respectively (Chow et al., 2004). Most of $\tau_{ATN,POC}$ should be attributed to the formation of POC, though the uncertainty in POC measurement by TOR or TOT and the variable mass absorption efficiency of POC prevents a strong correlation between $\tau_{ATN,POC}$ and POC (Chow et al., 2004).

Char was first quantified using the IMPROVE protocol as the low-temperature EC (EC1) minus POC, while the remaining high-temperature EC (EC2 + EC3) was attributed to soot (Han et al., 2007). The differentiation between char and soot has been applied to aerosol, dust, soil, and sediment samples (Han et al., 2009a; Jeong et al., 2013; Kim et al., 2011; Lim et al., 2012; Minoura et al., 2012) and validated with standard reference materials (SRMs) (Zhan et al., 2013).

The carbon concentrations of ambient $PM_{2.5}$ samples were reported in μg m^{-3}, while for the vegetation combustion samples the carbon concentrations were directly reported in μg cm^{-2} (of the filter), with no further calculations.

2.4. HULIS-C measurement

HULIS-C extraction follows Lin et al. (2010b) for both the ambient and source samples. A aliquot of filter (1.5−3 cm^2) was extracted with ultrapure water in an ultrasonic bath for 40 min and then filtered with a 0.45 μm Teflon syringe filter (Millipore, Billerica, MA) to remove the filter debris and suspended insoluble particles. The hydrochloric acid (HCl, 37%) was added to the extracts to reach pH = 2, then the acidified extracts were loaded on solid phase extraction (SPE) cartridges (Oasis HLB, 30 μm, 60 mg/cartridge, Waters, USA). HULIS, which are expected to be retained by the column, were eluted by 1.5 mL of methanol containing 2% aqueous ammonia (w/w). The resulting eluate was immediately evaporated to dryness under a gentle nitrogen (N_2) stream and redissolved in a known amount of ultrapure water. An aliquot of 5 μL extract was then spiked onto a prefired (850 °C for 3 h) quartz-fiber filter for quantification of HULIS-C by the DRI Model 2001 Carbon Analyzer. The HULIS-C concentrations reported here were corrected for method blank (~0.01 μg C μL^{-1}).

3. Comparison among IMPROVE, IMPROVE_A, and EUSAAR_2 analyses of ambient samples

As shown in Fig. S1, TC measurements were similar among the three protocols with correlation coefficients (r^2) >0.99 and near-unity slopes (0.97−1.03) for the 63 samples. This confirms homogeneous sample deposits and complete combustion, as observed in previous studies (Chow et al., 2001; Han et al., 2013).

Table 2
Statistical comparison of OC and EC measurements (units of μg m^{-3}) acquired in Xi'an during 2012–2013 (n = 63), using both reflectance and transmittance corrections (TOR and TOT) for the IMPROVE, IMPROVE_A, and EUSAAR_2 protocols.

Protocols		Orthogonal fit		Ordinary fit		t-test
x	y	Equation	r^2	with zero intercept	r^2	p[a]
OC						
IMPROVE TOR	IMPROVE_A TOR	y = 1.18x−1.02	0.99	y = 1.13x	0.99	0.22
IMPROVE TOR	EUSAAR_2 TOR	y = 0.91x+1.74	0.97	y = 0.99x	0.95	0.89
IMPROVE TOR	IMPROVE TOT	y = 1.27x−1.00	0.99	y = 1.22x	0.99	0.05
IMPROVE TOR	IMPROVE_A TOT	y = 1.40x−1.60	0.99	y = 1.32x	0.98	0.01
IMPROVE TOR	EUSAAR_2 TOT	y = 1.33x−0.72	0.98	y = 1.30x	0.98	0.01
IMPROVE_A TOR	EUSAAR_2 TOR	y = 0.77x+2.54	0.97	y = 0.87x	0.95	0.25
IMPROVE_A TOR	IMPROVE TOT	y = 1.07x+1.07	0.99	y = 1.07x	0.99	0.46
IMPROVE_A TOR	IMPROVE_A TOT	y = 1.18x−0.37	0.99	y = 1.17x	0.99	0.13
IMPROVE_A TOR	EUSAAR_2 TOT	y = 1.13x+0.46	0.98	y = 1.14x	0.98	0.15
EUSAAR_2 TOR	IMPROVE-TOT	y = 1.39x−3.50	0.96	y = 1.22x	0.95	0.06
EUSAAR_2 TOR	IMPROVE_A TOT	y = 1.54x−4.33	0.97	y = 1.33x	0.95	0.01
EUSAAR_2 TOR	EUSAAR_2 TOT	y = 1.46x−3.22	0.98	y = 1.30x	0.97	0.01
IMPROVE-TOT	IMPROVE_A TOT	y = 1.10x−0.38	0.99	y = 1.09x	0.99	0.42
IMPROVE-TOT	EUSAAR_2 TOT	y = 1.04x+0.58	0.98	y = 1.06x	0.98	0.49
EC						
IMPROVE TOR	IMPROVE_A TOR	y = 0.81x+0.43	0.94	y = 0.84x	0.94	0.17
IMPROVE TOR	EUSAAR_2 TOR	y = 1.09x−0.95	0.96	y = 1.01x	0.96	0.93
IMPROVE TOR	IMPROVE TOT	y = 0.57x+0.30	0.96	y = 0.60x	0.95	0.00
IMPROVE TOR	IMPROVE_A TOT	y = 0.45x+0.58	0.90	y = 0.49x	0.88	0.00
IMPROVE TOR	EUSAAR_2 TOT	y = 0.42x+0.41	0.83	y = 0.45x	0.82	0.00
IMPROVE_A TOR	EUSAAR_2 TOR	y = 1.34x−1.52	0.95	y = 1.19x	0.94	0.22
IMPROVE_A TOR	IMPROVE TOT	y = 0.70x+0.03	0.94	y = 0.70x	0.93	0.00
IMPROVE_A TOR	IMPROVE_A TOT	y = 0.56x+0.27	0.95	y = 0.58x	0.95	0.00
IMPROVE_A TOR	EUSAAR_2 TOT	y = 0.52x+0.12	0.86	y = 0.53x	0.86	0.00
EUSAAR_2 TOR	IMPROVE-TOT	y = 0.52x+0.85	0.92	y = 0.58x	0.90	0.00
EUSAAR_2 TOR	IMPROVE_A TOT	y = 0.41x+0.99	0.90	y = 0.48x	0.84	0.00
EUSAAR_2 TOR	EUSAAR_2 TOT	y = 0.39x+0.76	0.85	y = 0.44x	0.81	0.00
IMPROVE TOT	IMPROVE_A TOT	y = 0.79x+0.27	0.93	y = 0.83 x	0.92	0.10
IMPROVE TOT	EUSAAR_2 TOT	y = 0.75x+0.05	0.86	y = 0.75x	0.86	0.01

[a] p values of *t*-test for the ordinary fit with intercept through zero.

Table 2 shows good correlations of OC (r^2 = 0.95–0.99) and EC (r^2 = 0.81–0.96) among the three protocols, suggesting that regression coefficients may be used to estimate OC and EC from one to another protocol. However, EC concentrations varied by over two folds, whereas differences among the three protocols were smaller for OC (<33%) due to the relatively large fraction of OC in TC (see Table 2).

3.1. Temperature effects on the OC/EC split

Table 2 shows that the IMPROVE_A TOR EC is about 20% lower than the IMPROVE TOR EC. The higher IMPROVE_A temperatures also evolve ~20% more OC throughout the inert-atmosphere heating (i.e., OC1 + OC2 + OC3 + OC4) than the IMPROVE protocol while producing a similar amount of POC, as evidenced by similar levels of $\tau_{ATN,POC}$ between the two protocols (within 5% difference on average, see Fig. S2A). When implemented in the Model 2001 carbon analyzer, the IMPROVE peak inert atmospheric temperature (PIAT) appeared to be too low for completely evolving or pyrolyzing OC in these samples. OC being left over to the second stage of heating could inflate POC$_{R/T}$ or EC concentrations, depending on whether it was oxidatively-released before or after the optical split. This partly explains the higher TOR EC measured by the IMPROVE protocol than IMPROVE_A protocol. Such discrepancies did not occur when the IMPROVE protocol was implemented in the DRI/OGC analyzer since that combination would had produced higher heating temperatures (Chow et al., 2007).

The EUSAAR_2 protocol that has the highest PIAT of 650 °C and shortest heating time among the three protocols evolves slightly more OC than the IMPROVE_A protocol throughout its inert heating stage, according to the OC1-4 values (Fig. S3). It was noticed that filter reflectance started to increase in the EUSAAR_2 OC4 step for many samples. The increased sum of OC1-4, therefore, could result from oxidation of EC as the PIAT of EUSAAR_2 may be too high to keep EC intact under a trace level of oxygen in the OC heating stages (Chow et al., 2007). On the other hand, Chow et al. (2004) suggested that a higher heating rate in the inert atmosphere, like the one used by EUSSAR_2, can lead to more POC formation. The POC may be invisible for reflection detection as it is imbedded within the filter, and thus inflating the EC levels (Han et al., 2013). The coupling effect of this "premature" EC oxidation and excess POC formation on the OC/EC split point is complex. Better agreement was found for TOR EC between EUSAAR_2 and IMPROVE (y = 1.01 x) than between EUSAAR_2 and IMPROVE_A (y = 1.19x, Table 2). The IMPROVE and EUSAAR TOR EC are both higher than IMPROVE_A TOR EC but likely due to different reasons.

3.2. Influence of reflectance and transmittance adjustment on OC and EC determination

TOT EC was lower than TOR EC for each respective protocol, which could be attributed to the within-filter POC delaying the OC/EC split by transmittance much more than that by reflectance (Chow et al., 2004, 2001; Han et al., 2013). Ratios of EUSAAR_2 TOT to IMPROVE_A TOR were 1.14 for OC and 0.53 for EC (Table 2). As the within-filter POC increases with PIAT, TOT EC is expected to decrease with increasing PIAT (Subramanian et al., 2006). This study found the highest TOT EC (5.6 ± 3.3 μg m^{-3}) by IMPROVE and the lowest TOT EC (4.3 ± 2.6 μg m^{-3}) by EUSAAR_2, consistent with observation by Chow et al. (2001). However, for geological samples pretreated with acids to remove minerals and carbonate carbon, an

opposite trend was reported (Han et al., 2013), which may be associated with two competing effects caused by an increase in PIAT — one tends to increase the amount of POC, while the other causes more POC to evolve before EC (Cheng et al., 2012). The differences in TOT EC reached 25% among the three protocols.

Table 2 shows that EUSAAR_2 TOT EC is on average ~44% of its TOR EC. Discrepancies between TOR and TOT EC are smaller when measured by the IMPROVE and IMPROVE_A protocols (60% and 58%, respectively), with lower PIATs and an event driven heating duration (the temperature will not advance to next thermal fraction until the FID signal reaches baseline). On average, OC/EC ratios by TOT are 2.04 and 5.75 times the ratios by TOR for IMPROVE and EUSAAR_2, respectively. With the same reflectance or transmittance correction, the variation of PIAT produce different EC concentrations by 1–25%, while the alternation between reflectance and transmittance corrections with the same protocol can produce differences in EC concentrations of 40–56% (Table 1). The use of TOR or TOT adjustment appears to be the dominant factor influencing OC/EC split between the different protocols (e.g., IMPROVE/IMPROVE_A uses TOR and EUSAAR_2 uses TOT by default).

From the thermal analysis, good correlations ($r^2 = 0.60$–0.96) between TC and POC_R or POC_T from the three tested protocols (Fig. S4) suggest that pyrolizable organic compounds account for a certain fraction of carbonaceous aerosol in Xi'an. Large TC intercepts (-2.9–1.7 μg m^{-3}) in the POC-TC regressions (Fig. S4), i.e., higher than the corresponding sum of average OC1 and OC2, suggest that little POC is associated with OC1 and OC2 (i.e., <300 °C in the inert atmosphere). This is supported by the smallest changes in reflectance and transmittance during the OC1-2 steps.

4. Char and soot measured by different IMPROVE protocols

4.1. Protocol dependence of char and soot quantifications

Table 3 shows that IMPROVE and IMPROVE_A yield different char and soot concentrations. On average, char by IMPROVE_A TOR is ~87% of that by IMPROVE TOR, while soot by IMPROVE_A is only 60% of that by IMPROVE. As soot is the sum of EC2 and EC3, less soot would certainly be measured by IMPROVE_A with higher EC1 temperature and thus less carbon left.

There are strong correlations ($r^2 = 0.93$–0.96) between the char concentrations measured by the two protocols, though the correlation between soot concentrations was weak ($r^2 = 0.28$). The separation of char and soot is complicated for aerosol samples because the existence of oxidants and ions such as Fe_3O_4, MnO_2, and chloride ion could catalyze and accelerate the oxidation of carbon fractions. Soot oxidation is known to be promoted at low temperatures (i.e., <700 °C, the IMPROVE EC2 temperature) with

such catalysts (Han et al., 2009b; Novakov and Corrigan, 1995). This partly explains a poor correlation between the soot measurements by IMPROVE and IMPROVE_A. The correlations between soot and other carbon fractions (i.e., TC, OC, EC, and char) were also low. This is also consistent with the different sources of soot (i.e., from flaming fires via gas-to-particle conversion) from other fractions. Like EC, the IMPROVE char concentrations could be inflated by the uncertainties in OC/EC split. The IMPROVE TOR char are therefore higher than their corresponding IMPROVE_A TOR char.

4.2. Comparison of char and soot with HULIS-C

Fig. 1 shows moderate correlations of HULIS carbon with char and EC. With respect to the strength of correlation with HULIS, the order of TOR char > TOR EC > TOT char > TOT EC is found regardless of whether the IMPROVE or IMPROVE_A protocol is used. Char originates mainly from smoldering phases of biomass burning (Han et al., 2010), which is similar to those of HULIS (Graber and Rudich, 2006; Salma et al., 2010). Our finding is consistent with previous studies, which also showed good correlations of char with biomass burning markers such as potassium and levoglucosan (Lim et al., 2012; Minoura et al., 2012). Soot concentrations show no relationships with HULIS-C for both protocols ($r^2 = 0.03$, see Fig. 1 A3 and B3). This supports the differences in sources and formation pathways between HULIS and soot. Soot comes mainly from fossil fuel combustion, especially motor vehicle emissions in urban areas despite that flaming fire of biomass burning also contribute, while HULIS come mainly from smoldering fires as well as secondary organic aerosol formation. The poor correlations between soot and HULIS_C weaken the relations between EC and HULIS-C (Fig. 1).

5. Inter-protocol comparison of biomass combustion samples

OC dominated in TC (83–93%, see Table 4) from biomass combustion emissions, and strong correlations ($r^2 > 0.98$) of OC and TC concentrations were observed among the three different protocols. However, the EC relationships were weaker and variable, with correlation coefficients $r^2 = 0.56$–0.84 (Fig. 2A and B). Biomass combustion samples produced a relatively high proportion of volatile organics, chloride and potassium ions, and mineral dusts (Yokelson et al., 1997), which would catalyze the oxidation of EC on the filter (Han et al., 2009b; Novakov and Corrigan, 1995), leading to the premature evolution of EC. The relatively lower slopes of IMPROVE_A and EUSAAR_2 to IMPROVE EC (Fig. 2A and B) than those for ambient $PM_{2.5}$ samples (Table 2) may be associated with the faster oxidation of EC under higher temperatures with the presence of more oxidants. Ratios of IMPROVE TOR EC to EUSAAR_2 TOT EC produce a slope of 0.88 (Fig. 2A), which is slightly lower than that of the ambient samples (1.01 in Table 2).

Table 3
Statistical comparison of char and soot measurements (units of μg m^{-3}) acquired in Xi'an $PM_{2.5}$ during 2012–2013 for the IMPROVE and IMPROVE_A protocols using both reflectance and transmittance corrections.

Protocols		Orthogonal fit		Ordinary fit		t-test
x	y	Equation	r^2	through zero	r^2	p[a]
Char						
IMPROVE TOR	IMPROVE_A TOR	y = 0.82x+0.76	0.95	y = 0.87x	0.94	0.51
IMPROVE TOR	IMPROVE TOT	y = 0.57x−0.42	0.96	y = 0.53x	0.96	0.00
IMPROVE TOR	IMPROVE_A TOT	y = 0.44x+0.29	0.93	y = 0.47x	0.93	0.00
IMPROVE TOT	IMPROVE_A TOT	y = 0.79x+0.59	0.96	y = 0.88x	0.94	0.70
Soot[b]						
IMPROVE	IMPROVE_A	y = 0.68x−0.10	0.28	y = 0.61x	0.23	0.00

[a] p values of t-test for the ordinary fit with intercept through zero.
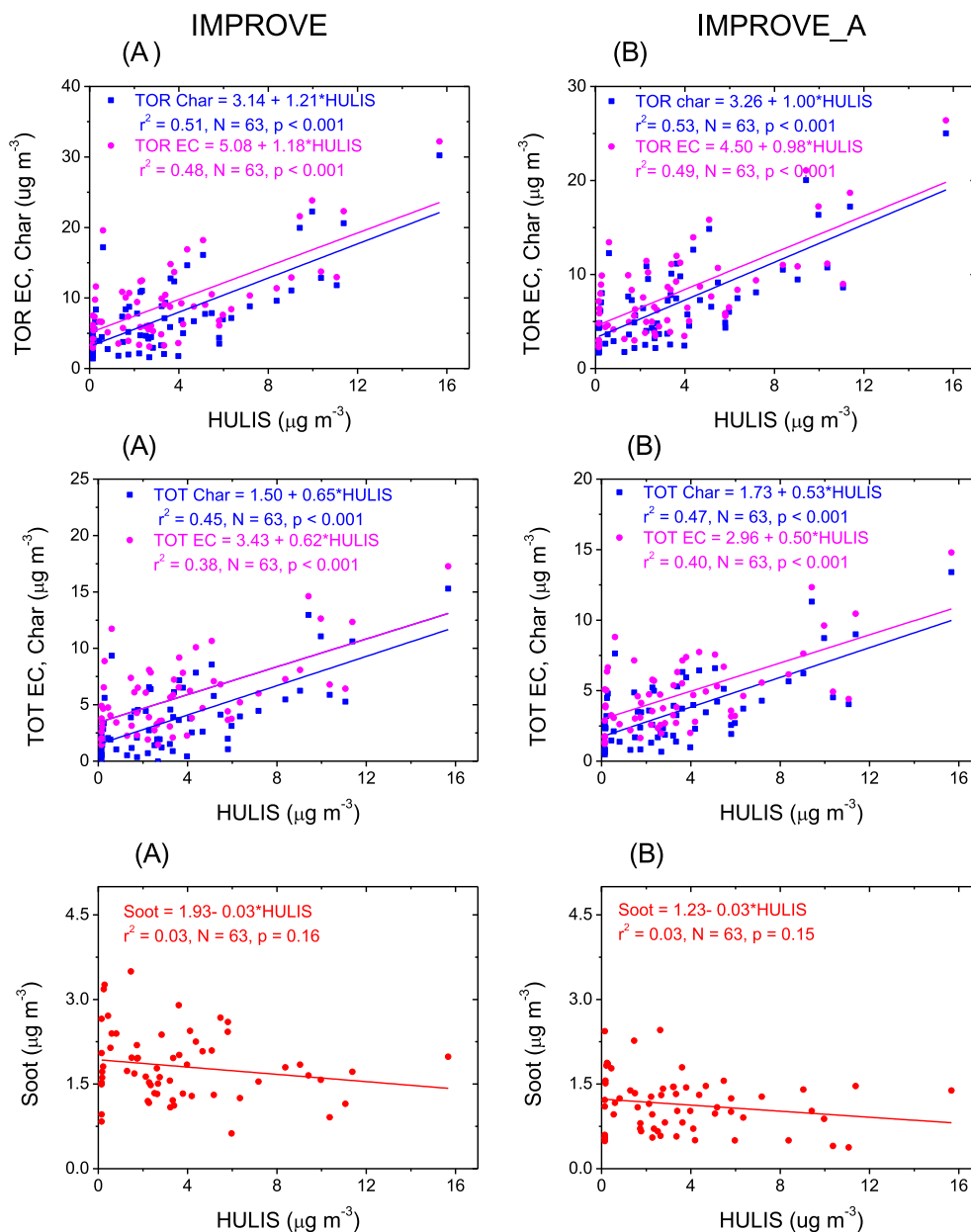[b] Soot is the sum of EC2 and EC3 with no reflectance or transmittance correction.

Fig. 1. Correlations between HULIS with EC, char, and soot measured with the IMPROVE and IMPROVE_A protocols, respectively, for the 63 ambient samples. (A1) HULIS versus IMPROVE TOR EC, and char, (A2) HULIS versus IMPROVE TOT EC, and char, (A3) HULIS versus IMPROVE soot, (B1) HULIS versus IMPROVE_A TOR EC, and char, (B2) HULIS versus IMPROVE_A TOT EC, and char, and (B3) HULIS versus IMPROVE_A soot.

Table 4
Summary of ratios of the carbon fractions for biomass combustion emissions (N = 20) under the flaming combustion (modified combustion efficiency >92%) in a laboratory combustion chamber.

	IMPROVE				IMPROVE_A				EUSAAR_2			
	Min.	Max.	Average	SD	Min.	Max.	Average	SD	Min.	Max.	Average	SD
TOR OC/TC (%)	75.7	91.5	82.5	0.04	76.5	93.4	86.1	0.05	78.3	89.3	84.7	0.04
TOR OC/EC	3.1	10.8	5.1	1.84	3.2	14.2	7.1	3.05	3.6	8.4	5.9	1.55
TOR Char/soot	1.4	17.3	5.8	3.84	1.0	124.0	23.0	33.8				
TOR Soot/EC (%)	11.2	25.0	18.8	0.10	0.8	50.5	17.0	0.14				
TOT OC/TC (%)	82.0	95.1	88.7	0.04	81.9	96.8	91.1	0.04	82.0	96.8	92.2	0.04
TOT OC/EC	4.6	19.3	8.7	3.36	4.5	30.1	12.7	6.79	4.6	29.9	14.9	6.97
TOT Char/soot	0.6	8.4	3.3	2.26	0.5	61.0	12.1	17.7				
TOT Soot/EC (%)	20.0	37.6	29.1	0.14	1.6	66.0	25.5	0.20				

Average char/soot ratios ranged from 1.4 to 17.3 (average = 5.8)   using the IMPROVE TOR protocol, which is within the range of the
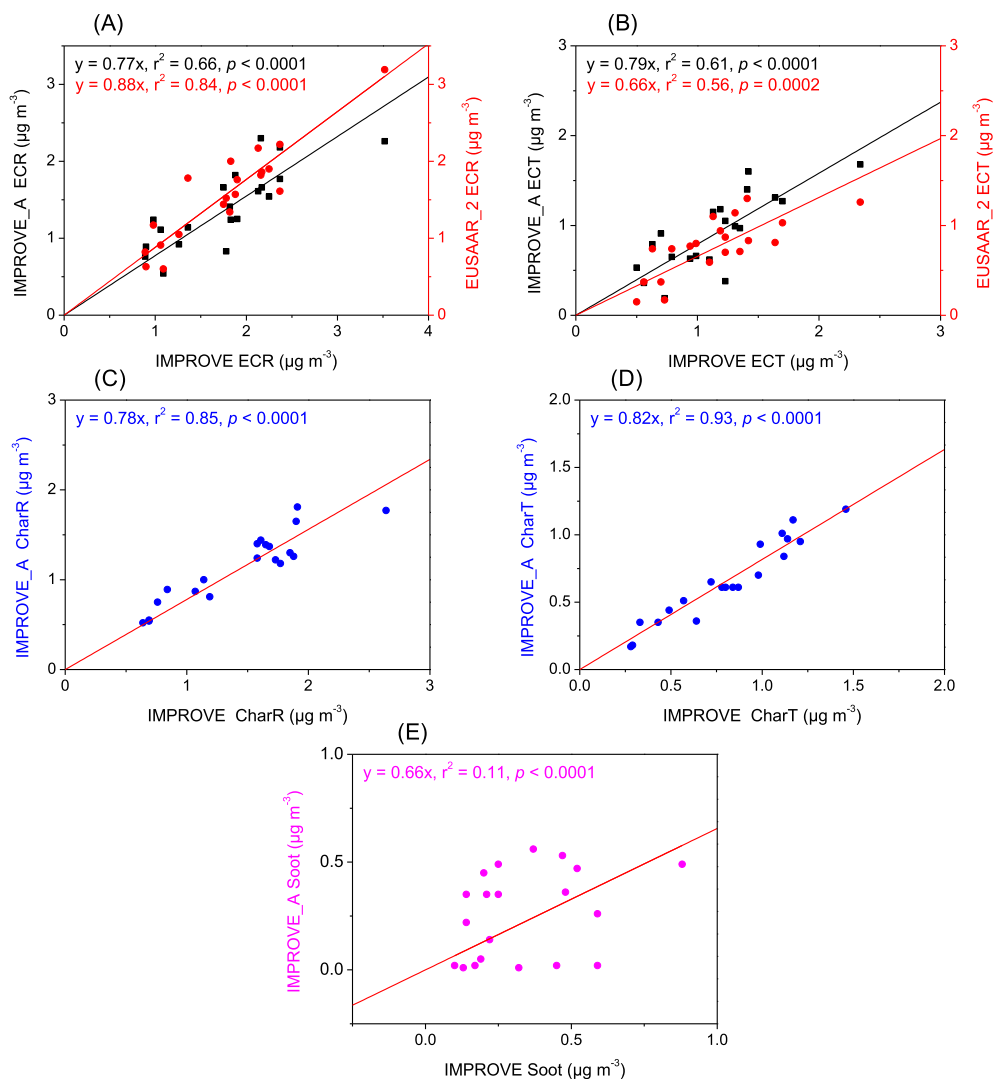
Fig. 2. Comparison of different carbon fractions measured using the three protocols (IMPROVE, IMPROVE_A, and EUSAAR_2) with the TOR and TOT corrections for 20 biomass combustion samples. (A) IMPROVE TOR EC vs IMPROVE_A and EUSAAR_2 TOR EC, (B) IMPROVE TOT EC vs IMPROVE_A and EUSAAR_2 TOT EC, (C) IMPROVE TOR char vs IMPROVE_A TOR char, (D) IMPROVE TOT char vs IMPROVE_A TOT char, and (E) IMPROVE soot vs IMPROVE_A soot.

Table 5
Summary of the concentrations of the carbon fractions ($\mu g\ m^{-3}$) in $PM_{2.5}$ (N = 63) in Xi'an, China, measured using the three different protocols.

	IMPROVE					IMPROVE_A					EUSAAR_2				
	Min.	Max.	Average	SD	CV	Min.	Max.	Average	SD	CV	Min.	Max.	Average	SD	CV
TC $\mu g\ m^{-3}$	10.04	84.20	26.79	14.60	0.54	10.22	90.20	27.67	15.10	0.55	9.73	83.87	26.91	14.28	0.53
TOR OC $\mu g\ m^{-3}$	7.11	51.99	17.52	9.08	0.52	7.26	63.80	19.69	10.72	0.54	7.32	51.69	17.73	8.30	0.47
TOR POC $\mu g/m^3$	1.13	19.28	4.85	3.80	0.78	0.95	26.11	4.85	4.46	0.92	0.00	13.17	1.29	2.30	1.78
TOR EC $\mu g\ m^{-3}$	2.93	32.21	9.27	5.72	0.62	2.28	26.40	7.97	4.68	0.59	2.41	32.18	9.18	6.24	0.68
TOR OC/EC	1.36	3.66	2.04	0.48	0.24	1.67	4.90	2.64	0.71	0.27	1.18	4.05	2.23	0.64	0.29
TOT POC $\mu g/m^3$	2.36	34.21	8.49	6.15	0.72	2.11	37.72	8.09	6.39	0.79	1.29	33.72	6.26	5.84	0.93
TOT OC $\mu g\ m^{-3}$	8.58	66.92	21.16	11.47	0.54	8.53	75.41	22.92	12.67	0.55	8.52	72.25	22.62	12.05	0.53
TOT EC $\mu g\ m^{-3}$	1.45	17.28	5.62	3.32	0.59	1.23	14.79	4.74	2.66	0.56	1.21	11.62	4.29	2.55	0.59
TOT OC/EC	2.28	6.74	4.06	0.97	0.24	3.07	9.19	5.14	1.43	0.28	1.63	9.88	5.75	1.42	0.25
TOR Char $\mu g\ m^{-3}$	1.41	30.22	7.45	5.68	0.76	1.69	25.01	6.83	4.66	0.68					
TOT Char $\mu g\ m^{-3}$	−0.07	15.29	3.81	3.25	0.853	0.47	13.40	3.60	2.58	0.72					
Soot $\mu g\ m^{-3}$	0.62	3.50	1.82	0.60	0.33	0.38	2.46	1.14	0.49	0.43					
TOR Char/soot	0.92	15.23	4.55	3.67	0.81	1.26	26.70	7.29	6.01	0.82					
TOT Char/soot	−0.05	7.84	2.31	2.04	0.88	0.38	11.31	3.75	3.02	0.81					

reported char/soot ratios for biomass burning samples (Han et al., 2010). However, because the samples used in this study were collected from laboratory-based flaming combustion with high

modified combustion efficiencies (MCE > 92%, measured during the sample collection period using real-time CO and CO_2 detectors (Tian et al., 2015)), they were likely to differ from emissions from

suppressed burning, domestic heating, and cooking, which may have relatively higher char/soot ratios due to their lower MCE.

As the PIAT increases from IMPROVE to IMPROVE_A, it lowers the char and soot concentrations and increases char/soot ratios (Tables 4 and 5). Lower soot concentrations can be attributed to two reasons: (1) the higher EC1 temperature leading to more carbon evolved in OC and EC1 steps and thus resulting in lower soot yields, and (2) a catalytic effect of soot (Ishiguro et al., 1997) due to the higher temperature in IMPROVE_A EC1 step that would misclassify soot as POC or char. The IMPROVE and IMPROVE_A soot concentrations are poorly correlated ($r^2 = 0.11$; see Fig. 2). This raises concerns over the char and soot differentiation by different protocols.

6. Variations of ambient PM$_{2.5}$ carbon fractions in Xi'an over one year

Table 5 presents the summarized statistics for the carbon fractions of PM$_{2.5}$ in Xi'an measured with the three protocols. The annual average PM$_{2.5}$ mass concentration was 134 ± 80 µg m^{-3} (average $\pm$ standard deviation), which is much higher than the Chinese air pollution standard of 35 µg m^{-3}, the National Ambient Air Quality Guideline of the European Union (25 µg m^{-3}), and the World Health Organization (WHO) Air Quality Guideline of 10 µg m^{-3}. Annual average TC concentration (26.8–27.7 µg m^{-3} measured by different protocols, Table 5) alone would be close to the Chinese PM$_{2.5}$ standard and exceeds the US EPA PM$_{2.5}$ standard of 12 µg m^{-3}. Compared with the 2004 data (Han et al., 2010), however, PM$_{2.5}$ mass and TC concentrations have decreased by ~25% and ~40%, respectively. This is likely, in addition to the meteorological variability, a consequence of pollution control measures made by the local government (Table S1). With the implementation of the new Prevention and Control of Atmospheric Pollution Act of China in 2000 (Cao, 2014), most of chemical factories, coal-fired power plants, and heavy industrials have gradually been moved out from Xi'an. Moreover, with the establishment of the Chinese PM$_{2.5}$ pollution standard in 2011, more strong pollution control measures have been enforced by local governments. It was demonstrated that both a stagnant weather condition and the prevailing East Asian Monsoon (EAM) could impact air quality in the region, although the EAM pattern has not varied much between 2004 and 2013 in northern China (Zhang et al., 2016).

Temporal variations in TC, OC, EC, char and soot concentrations as well as their ratios are shown in Fig. 3. Similar to mass variations, TC, OC, EC, and char all displayed higher winter and lower summer concentrations. This pattern is common in north China (Cao, 2014; Huang et al., 2014) due to the heating season in winter, along with the decrease of boundary layer depth as the temperature cools down. Soot concentrations did not display a clear seasonal variation (Fig. 3). This is consistent with our previous study of soot distributions in 14 Chinese cities (Han et al., 2009c), and it was explained by the regional atmospheric transport of submicron soot particles (Masiello, 2004). This phenomenon has also been reported by Jeong et al. (2013) in North America, through a comparison of daily soot levels in urban and rural areas.

Char/soot ratios are generally >3 in biomass burning and coal combustion samples, while those of motor vehicle exhausts have char/soot ratios <1.0 (Han et al., 2010). The difference in char/soot ratios of different emission sources is reflected in the change of energy structure in Xi'an. It is noted that the average soot concentration of this study is 1.82 ± 0.60 µg m^{-3} (Table S1), higher than 1.54 ± 0.64 µg m^{-3} in 2004 using IMPROVE protocol (Han et al., 2010). This is likely associated with increase in vehicular fleets from 3.1×10^5 in 2004 to 16.1×10^5 in 2012, though the vehicle

emission standards have been greatly improved. However, the char concentration decreased from 6.8 µg m^{-3} in 2004 (Han et al., 2010) to 3.8 µg m^{-3} in 2012−2013 (this study) by the IMPROVE TOT protocol due to the great efforts by the local government to reduce biomass burning in the surrounding rural areas and relocation of coal-fired boilers in recent year. Correspondingly, OC/EC ratios also decrease from 4.6 in 2004 to 4.1 in 2012−2013 (Table S1), which is far lower than the decrease of char/soot ratios. Ratio of soot to EC exceeded 50% in summer (using the IMPROVE TOR method; the fraction was even higher using IMPROVE TOT protocol). Soot fraction can be as low as 6.2% in EC for winter days. These proportions are comparable with the results of a recent study in a rural area of Europe that used the chemothermal CTO-375 method for soot determination (Pohl et al., 2014). The highest char concentrations (using IMPROVE TOR protocol) occurred in winter, and were over 10 µg m^{-3}, accounting for 80−90% of EC and highlighting the importance of reducing char emissions on local pollution control and climatic forcing in western China, where solid fuels are still the main energy source for winter heating (Zhang et al., 2009).

Both OC/EC and char/soot ratios have been used for identifying sources of carbonaceous aerosol (Cao et al., 2003; Castro et al., 1999; Han et al., 2010). The formation of secondary organic aerosol (SOA) can influence the atmospheric OC concentrations, and thus modify the OC/EC ratio from primary emissions (Jimenez et al., 2009). However, the char/soot ratio from a primary source should be conserved in the atmosphere. In this study, the OC/EC ratio shows peaks in both summer and winter, while the char/soot ratio shows single peak in winter. The summer peak in the OC/EC ratio can thus be explained by the SOA formation (Huang et al., 2014) and the increasing contribution from biomass burning emissions (Zhang et al., 2014). The vehicular emissions would dominate EC in summer, which is confirmed by the low char/soot ratios (Fig. 3).

The char/soot ratio is useful for source identification. The IMPROVE and IMPROVE_A (using TOR or TOT) produce different char and soot concentrations and their ratios, which would affect source identification. The low-temperature IMPROVE protocol generally produces lower char/soot ratios than those of IMPROVE_A protocol, with the lowest and highest annual char/soot ratio of 2.3 by the IMPROVE TOT and of 7.3 by the IMPROVE_A TOR (see Table 5).

HULIS-C concentrations over the one-year sampling period averaged 4.27 µg m^{-3}, accounting for 27.7% of TC, comparable with other studies in China (Lin et al., 2010a). If we assume the OM/OC ratio of 2.0 for HULIS suggested by Polidori et al. (2008), the proportion of HULIS in PM$_{2.5}$, on average, is ~9.6%. Overall HULIS-C concentrations showed a temporal pattern similar to char and EC concentrations (Fig. 4), with higher winter and lower summer and spring concentrations. This supports the contribution of HULIS from biomass burning. Zhang et al. (2014) showed that the concentrations of levoglucosan, a tracer of biomass burning emissions, in Xi'an during winter and fall can be 1-2 orders of magnitude higher than those in summer. The main contribution comes from domestic biomass burning for heating instead of open fire. However, the HULIS-C/TC and HULIS/mass ratios did not peak in winter. This implies other important sources of HULIS, most likely SOA, in summer (Lin et al., 2010a), which is consistent with the high OC/EC ratios in summer compared with those in spring and fall (Fig. 3).

7. Implications

Because OC/EC ratios determine the relative contribution of particle scattering and absorption, they are often used to estimate the radiative forcing of carbonaceous aerosols (Novakov et al., 2005). Comparisons of the routine protocols IMPROVE, IMPROVE_A, and EUSAAR_2 show a large difference (a factor of 2.7) in OC/
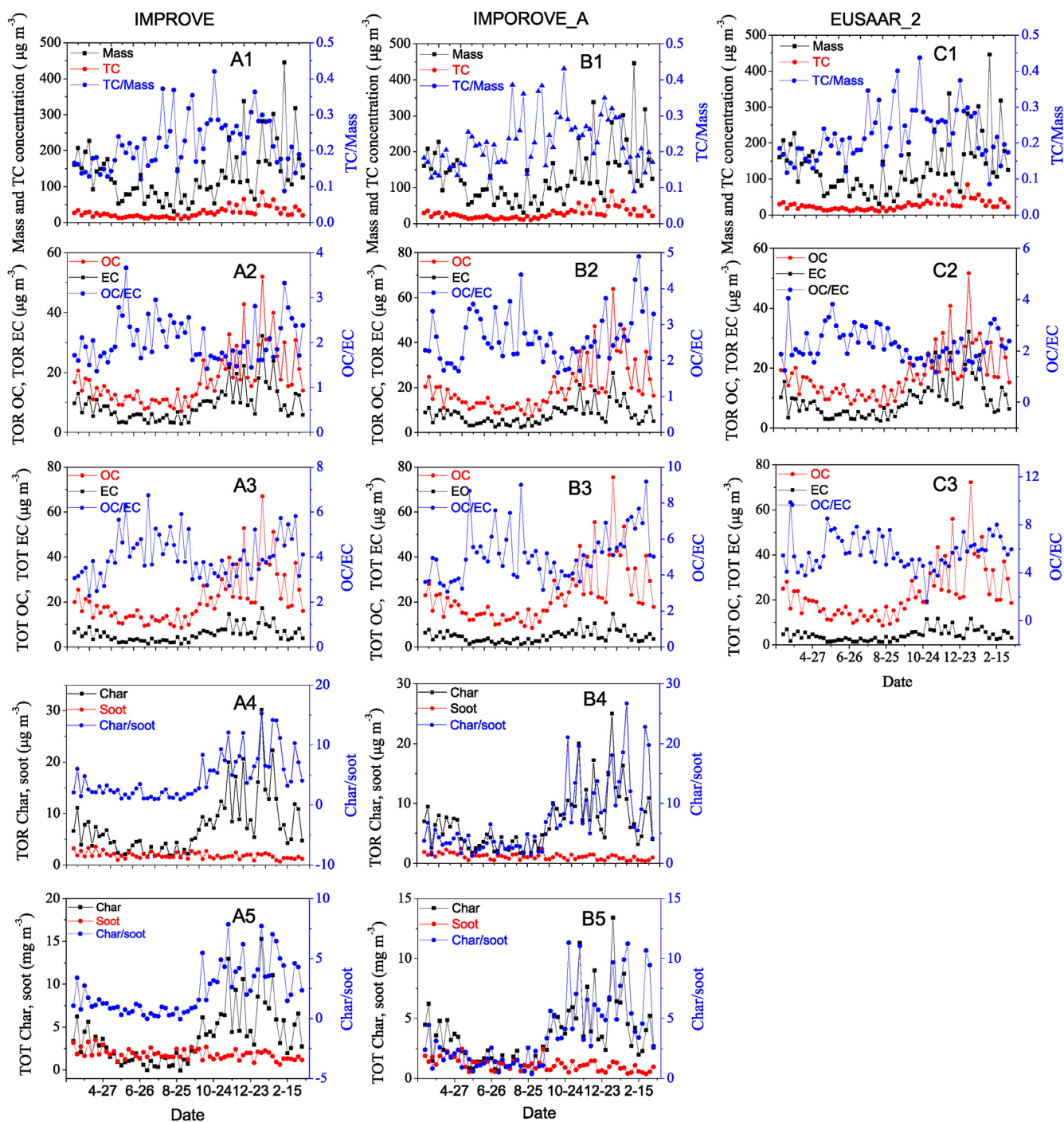
Fig. 3. Variations of mass concentration and carbon fractions and their ratios in PM$_{2.5}$ of Xi'an city during 2012–2013 using the three protocols (IMPROVE, IMPROVE_A, and EUSAAR_2). (1) A1, B1, and C1, TC and mass concentrations, and their ratios; (2) A2, B2, and C2, TOR OC and EC, and their ratios measured with the three protocols; (3) A3, B3, and C3, TOT OC and EC, and their ratios measured with the three protocols; (4) A4 and B4, TOR char and soot, and their ratios measured with the IMPROVE and IMPROVE_A protocols; and (5) A5 and B5, TOT char and soot, and their ratios measured with the IMPROVE and IMPROVE_A protocols.

EC ratios among the protocols. Current models based on aerosol observations and emission inventories may have a potential uncertainty of more than a factor of two when estimating the radiative forcing of carbonaceous aerosols (Sato et al., 2003), which can be partly explained by the differences from OC/EC measurement using the different protocols. Average PM$_{2.5}$ OC/EC ratio in Xi'an during 2012–2013 is ~2.0 using the IMPROVE TOR protocol, in comparison with ~5.7 using the EUSSAR II TOT protocol. Higher IMPROVE TOR

EC by IMPROVE protocol would suggest higher warming effects than those of EUSAAR_2 protocol. Direct measurements of aerosol optical properties from primary sources, in conjunction with the OC/EC analysis, can help reduce the uncertainty by recommending the appropriate mass absorption efficiencies of EC in the climate models.

High correlations of OC or EC concentrations determined by the different TO protocols suggest the possibility of reconciling
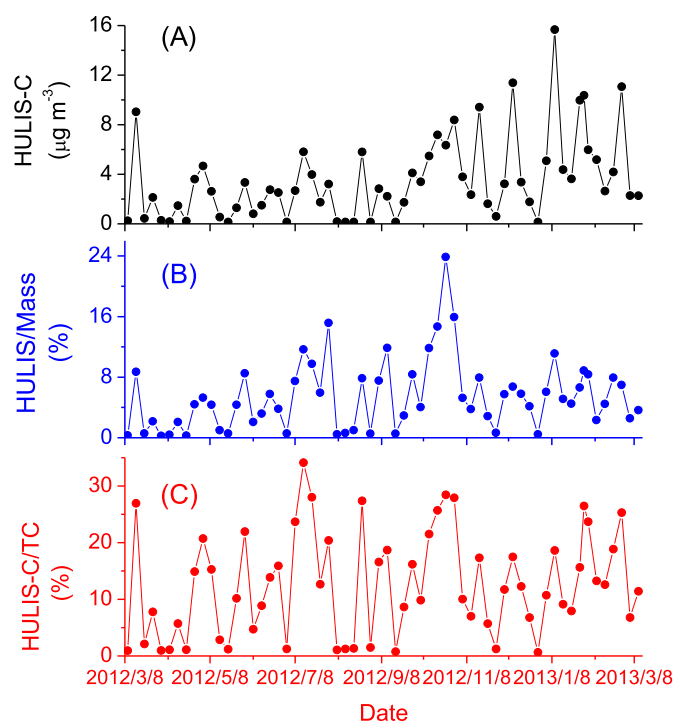
Fig. 4. Time series of (A) HULIS-C concentration, (B) HULIS/mass, and (C) HULIS-C/TC in PM$_{2.5}$ of Xi'an, China during 2012–2013. Note: HULIS concentrations in (B) are estimated using the ratio of OM/OC of 2.0 suggested by Polidori et al. (2008).

protocol-specific measurements into a common database. An approach would involve reanalyzing a subset of samples using reference protocol(s) such as the IMPROVE_A protocol, which has long been used for carbonaceous aerosol measurement, and has documented more than 200,000 sample data. Such reconciliations should be considered for previous datasets if samples have been adequately archived in cold (<−20 °C) stage.

Char and soot have different physico-chemical and optical properties. Char is likely to be less light-absorbing than soot, and future studies should distinguish the atmospheric distribution and radiative forcing of the two EC subtypes. However, since the char/soot split is sensitive to the TO protocol used, caution should be made when applying different TO protocols. In addition, the aerosol matrix can influence the TO analysis, and therefore future studies may consider approaches to simplify the aerosol matrix such as removing water-soluble ions, metal oxides, and carbonate prior to TO analysis. With the rapid economic development of China and the increasing motor vehicle emissions, an increase in soot and decrease in char would be expected, and such trend has been occurred in the past decade in Xi'an. The potential effects of such shift on climate should get more attention.

Acknowledgement

Appendix A. Supplementary data

Supplementary data related to this article can be found at http://dx.doi.org/10.1016/j.atmosenv.2016.02.023

References

Andreae, M.O., Gelencser, A., 2006. Black carbon or brown carbon? the nature of light-absorbing carbonaceous aerosols. Atmos. Chem. Phys. 6, 3131–3148.

Asa-Awuku, A., Sullivan, A.P., Hennigan, C.J., Weber, R.J., Nenes, A., 2008. Investigation of molar volume and surfactant characteristics of water-soluble organic compounds in biomass burning aerosol. Atmos. Chem. Phys. 8, 799–812.

Birch, M.E., Cary, R.A., 1996. Elemental carbon-based method for monitoring occupational exposures to particulate diesel exhaust. Aerosol Sci. Technol. 25, 221–241.

Bond, T.C., Doherty, S.J., Fahey, D.W., Forster, P.M., Berntsen, T., DeAngelo, B.J., Flanner, M.G., Ghan, S., Kaercher, B., Koch, D., Kinne, S., Kondo, Y., Quinn, P.K., Sarofim, M.C., Schultz, M.G., Schulz, M., Venkataraman, C., Zhang, H., Zhang, S., Bellouin, N., Guttikunda, S.K., Hopke, P.K., Jacobson, M.Z., Kaiser, J.W., Klimont, Z., Lohmann, U., Schwarz, J.P., Shindell, D., Storelvmo, T., Warren, S.G., Zender, C.S., 2013. Bounding the role of black carbon in the climate system: a scientific assessment. J. Geophys. Res. 118, 5380–5552.

Cao, J.J., 2014. PM2.5 and Environment. Science Press, Beijing.

Cao, J.J., Lee, S.C., Chow, J.C., Watson, J.G., Ho, K.F., Zhang, R.J., Jin, Z.D., Shen, Z.X., Chen, G.C., Kang, Y.M., Zou, S.C., Zhang, L.Z., Qi, S.H., Dai, M.H., Cheng, Y., Hu, K., 2007. Spatial and seasonal distributions of carbonaceous aerosols over China. J. Geophys. Res. 112 http://dx.doi.org/10.1029/2006jd008205.

Cao, J.J., Lee, S.C., Ho, K.F., Zhang, X.Y., Zou, S.C., Fung, K., Chow, J.C., Watson, J.G., 2003. Characteristics of carbonaceous aerosol in Pearl River Delta Region, China during 2001 winter period. Atmos. Environ. 37, 1451–1460.

Cao, J.J., Zhu, C.S., Tie, X.X., Geng, F.H., Xu, H.M., Ho, S.S.H., Wang, G.H., Han, Y.M., Ho, K.F., 2013. Characteristics and sources of carbonaceous aerosols from Shanghai, China. Atmos. Chem. Phys. 13, 803–817.

Castro, L.M., Pio, C.A., Harrison, R.M., Smith, D.J.T., 1999. Carbonaceous aerosol in urban and rural European atmospheres: estimation of secondary organic carbon concentrations. Atmos. Environ. 33, 2771–2781.

Cavalli, F., Viana, M., Yttri, K.E., Genberg, J., Putaud, J.P., 2010. Toward a standardised thermal-optical protocol for measuring atmospheric organic and elemental carbon: the EUSAAR protocol. Atmos. Meas. Tech. 3, 79–89.

Chameides, W.L., Bergin, M., 2002. Climate change – soot takes center stage. Science 297, 2214–2215.

Chen, L.W.A., Chow, J.C., Watson, J.G., Moosmuller, H., Arnott, W.P., 2004. Modeling reflectance and transmittance of quartz-fiber filter samples containing elemental carbon particles: implications for thermal/optical analysis. J. Aerosol Sci. 35, 765–780.

Cheng, Y., Duan, F.-k., He, K.-b., Du, Z.-y., Zheng, M., Ma, Y.-l., 2012. Intercomparison of thermal-optical method with different temperature protocols: Implications from source samples and solvent extraction. Atmos. Environ. 61, 453–462.

Chow, J.C., Watson, J.G., Chen, L.W.A., Arnott, W.P., Moosmuller, H., 2004. Equivalence of elemental carbon by thermal/optical reflectance and transmittance with different temperature protocols. Environ. Sci. Technol. 38, 4414–4422.

Chow, J.C., Watson, J.G., Chen, L.W.A., Chang, M.CO., Robinson, N.F., Trimble, D., Kohl, S., 2007. The IMPROVE-A temperature protocol for thermal/optical carbon analysis: maintaining consistency with a long-term database. J. Air Waste Manag. 57, 1014–1023.

Chow, J.C., Watson, J.G., Crow, D., Lowenthal, D.H., Merrifield, T., 2001. Comparison of IMPROVE and NIOSH carbon measurements. Aerosol Sci. Technol. 34, 23–34.

Chow, J.C., Watson, J.G., Louie, P.K.K., Chen, L.W.A., Sin, D., 2005. Comparison of PM2.5 carbon measurement methods in Hong Kong, China. Environ. Pollut. 137, 334–344.

Chow, J.C., Watson, J.G., Pritchett, L.C., Pierson, W.R., Frazier, C.A., Purcell, R.G., 1993. The dri thermal/optical reflectance carbon analysis system: description, evaluation and applications in U.S. Air quality studies. Atmos. Environ. Part A. General Top. 27, 1185–1201.

CNEMC, 2013. China National Environmental Monitoring Centre, Air Quality Report in 74 Chinese Cities in March and the First Quarter 2013. http://www.cnemc.cn/publish/106/news/news_34605.html (in Chinese), accessed on34611 June 32013).

Goldberg, E.D., 1985. Black Carbon in the Environment. John Wiley & Sons, Inc., New York.

Graber, E.R., Rudich, Y., 2006. Atmospheric HULIS: how humic-like are they? A comprehensive and critical review. Atmos. Chem. Phys. 6, 729–753.

Gray, H.A., Cass, G.R., Huntzicker, J.J., Heyerdahl, E.K., Rau, J.A., 1984. Elemental and organic-carbon particle concentrations – a long-term perspective. Sci. Total Environ. 36, 17–25.

Hammes, K., Schmidt, M.W.I., Smernik, R.J., Currie, L.A., Ball, W.P., Nguyen, T.H., Louchouarn, P., Houel, S., Gustafsson, O., Elmquist, M., Cornelissen, G., Skjemstad, J.O., Masiello, C.A., Song, J., Peng, P.a., Mitra, S., Dunn, J.C., Hatcher, P.G., Hockaday, W.C., Smith, D.M., Hartkopf-Froeder, C., Boehmer, A., Lueer, B., Huebert, B.J., Amelung, W., Brodowski, S., Huang, L., Zhang, W., Gschwend, P.M., Flores-Cervantes, D.X., largeau, C., Rouzaud, J.-N., Rumpel, C., Guggenberger, G., Kaiser, K., Rodionov, A., Gonzalez-Vila, F.J., Gonzalez-Perez, J.A., de la Rosa, J.M., Manning, D.A.C., Lopez-Capel, E., Ding, L., 2007. Comparison of quantification methods to measure fire-derived (black/elemental) carbon in soils and sediments using reference materials from soil, water, sediment and the atmosphere. Glob. Biogeochem. Cycles 21.

Han, Y., Chen, A., Cao, J., Fung, K., Ho, F., Yan, B., Zhan, C., Liu, S., Wei, C., An, Z., 2013. Thermal/optical methods for elemental carbon quantification in soils and urban dusts: equivalence of different analysis protocols. PLoS One 8.

Han, Y.M., Cao, J.J., Chow, J.C., Watson, J.G., An, Z.S., Jin, Z.D., Fung, K.C., Liu, S.X., 2007. Evaluation of the thermal/optical reflectance method for discrimination between char- and soot-EC. Chemosphere 69, 569–574.

Han, Y.M., Cao, J.J., Chow, J.C., Watson, J.G., An, Z.S., Liu, S.X., 2009a. Elemental carbon in urban soils and road dusts in Xi'an, China and its implication for air pollution. Atmos. Environ. 43, 2464–2470.

Han, Y.M., Cao, J.J., Lee, S.C., Ho, K.F., An, Z.S., 2010. Different characteristics of char and soot in the atmosphere and their ratio as an indicator for source identification in Xi'an, China. Atmos. Chem. Phys. 10, 595–607.

Han, Y.M., Cao, J.J., Posmentier, E.S., Chow, J.C., Watson, J.G., Fung, K.K., Jin, Z.D., Liu, S.X., An, Z.S., 2009b. The effect of acidification on the determination of elemental carbon, char-, and soot-elemental carbon in soils and sediments. Chemosphere 75, 92–99.

Han, Y.M., Lee, S.C., Cao, J.J., Ho, K.F., An, Z.S., 2009c. Spatial distribution and seasonal variation of char-EC and soot-EC in the atmosphere over China. Atmos. Environ. 43, 6066–6073.

Hitzenberger, R., Petzold, A., Bauer, H., Ctyroky, P., Pouresmaeil, P., Laskus, L., Puxbaum, H., 2006. Intercomparison of thermal and optical measurement methods for elemental carbon and black carbon at an urban location. Environ. Sci. Technol. 40, 6377–6383.

Hitzenberger, R., Tohno, S., 2001. Comparison of black carbon (BC) aerosols in two urban areas - concentrations and size distributions. Atmos. Environ. 35, 2153–2167.

Hoffer, A., Gelencser, A., Guyon, P., Kiss, G., Schmid, O., Frank, G.P., Artaxo, P., Andreae, M.O., 2006. Optical properties of humic-like substances (HULIS) in biomass-burning aerosols. Atmos. Chem. Phys. 6, 3563–3570.

Huang, R.-J., Zhang, Y., Bozzetti, C., Ho, K.-F., Cao, J.-J., Han, Y., Daellenbach, K.R., Slowik, J.G., Platt, S.M., Canonaco, F., Zotter, P., Wolf, R., Pieber, S.M., Bruns, E.A., Crippa, M., Ciarelli, G., Piazzalunga, A., Schwikowski, M., Abbaszade, G., Schnelle-Kreis, J., Zimmermann, R., An, Z., Szidat, S., Baltensperger, U., El Haddad, I., Prevot, A.S.H., 2014. High secondary aerosol contribution to particulate pollution during haze events in China. Nature 514, 218–222.

Ishiguro, T., Takatori, Y., Akihama, K., 1997. Microstructure of diesel soot particles probed by electron microscopy: first observation of inner core and outer shell. Combust. Flame 108, 231–234.

Jacobson, M.Z., 2001. Strong radiative heating due to the mixing state of black carbon in atmospheric aerosols. Nature 409, 695–697.

Janssen, N.A.H., Gerlofs-Nijland, M.E., Lanki, T., Salonen, R.O., Cassee, F., Hoek, G., Fischer, P., Brunekreef, B., Krzyzanowski, M., 2012. Health Effects of Black Carbon, World Health Organization Report. WHO Regional Office for Europe, Copenhagen, Denmark.

Jeong, C.-H., Herod, D., Dabek-Zlotorzynska, E., Ding, L., McGuire, M.L., Evans, G., 2013. Identification of the sources and geographic origins of black carbon using factor analysis at paired rural and urban sites. Environ. Sci. Technol. 47, 8462–8470.

Jimenez, J., Canagaratna, M., Donahue, N., Prevot, A., Zhang, Q., Kroll, J., DeCarlo, P., Allan, J., Coe, H., Ng, N., 2009. Evolution of organic aerosols in the atmosphere. Science 326, 1525–1529.

Kim, K.H., Sekiguchi, K., Furuuchi, M., Sakamoto, K., 2011. Seasonal variation of carbonaceous and ionic components in ultrafine and fine particles in an urban area of Japan. Atmos. Environ. 45, 1581–1590.

Lim, S., Lee, M., Lee, G., Kim, S., Yoon, S., Kang, K., 2012. Ionic and carbonaceous compositions of PM10, PM2.5 and PM1.0 at Gosan ABC Superstation and their ratios as source signature. Atmos. Chem. Phys. 12, 2007–2024.

Lin, P., Engling, G., Yu, J.Z., 2010a. Humic-like substances in fresh emissions of rice straw burning and in ambient aerosols in the Pearl River Delta Region, China. Atmos. Chem. Phys. 10, 6487–6500.

Lin, P., Huang, X.-F., He, L.-Y., Yu, J.Z., 2010b. Abundance and size distribution of HULIS in ambient aerosols at a rural site in South China. J. Aerosol Sci. 41, 74–87.

Masiello, C.A., 2004. New directions in black carbon organic geochemistry. Mar. Chem. 92, 201–213.

Mauderly, J.L., Chow, J.C., 2008. Health effects of organic aerosols. Inhal. Toxicol. 20, 257–288.

Mayol-Bracero, O.L., Guyon, P., Graham, B., Roberts, G., Andreae, M.O., Decesari, S., Facchini, M.C., Fuzzi, S., Artaxo, P., 2002. Water-soluble organic compounds in biomass burning aerosols over Amazonia – 2. Apportionment of the chemical composition and importance of the polyacidic fraction. J. Geophys. Res. 107.

Minoura, H., Morikawa, T., Mizohata, A., Sakamoto, K., 2012. Carbonaceous aerosol and its characteristics observed in Tokyo and south Kanto region. Atmos. Environ. 61, 605–613.

Novakov, T., Corrigan, C.E., 1995. Thermal characterization of biomass smoke particles. Mikrochim. Acta 119, 157–166.

Novakov, T., Menon, S., Kirchstetter, T.W., Koch, D., Hansen, J.E., 2005. Aerosol organic carbon to black carbon ratios: analysis of published data and implications for climate forcing. J. Geophys. Res. 110. D21205.

Pohl, K., Cantwell, M., Herckes, P., Lohmann, R., 2014. Black Carbon Concentrations and Sources in the Marine Boundary Layer of the Tropical Atlantic Ocean Using Four Methodologies. Copernicus GmbH, pp. 29785–29810.

Polidori, A., Turpin, B.J., Davidson, C.I., Rodenburg, L.A., Maimone, F., 2008. Organic PM 2.5: fractionation by polarity, FTIR spectroscopy, and OM/OC ratio for the Pittsburgh aerosol. Aerosol Sci. Technol. 42, 233–246.

Ramanathan, V., Carmichael, G., 2008. Global and regional climate changes due to black carbon. Nat. Geosci. 1, 221–227.

Reisinger, P., Wonaschuetz, A., Hitzenberger, R., Petzold, A., Bauer, H., Jankowski, N., Puxbaum, H., Chi, X., Maenhaut, W., 2008. Intercomparison of measurement techniques for black or elemental carbon under urban background conditions in wintertime: influence of biomass combustion. Environ. Sci. Technol. 42, 884–889.

Saleh, R., Robinson, E.S., Tkacik, D.S., Ahern, A.T., Liu, S., Aiken, A.C., Sullivan, R.C., Presto, A.A., Dubey, M.K., Yokelson, R.J., 2014. Brownness of organics in aerosols from biomass burning linked to their black carbon content. Nat. Geosci. 7, 647–650.

Salma, I., Meszaros, T., Maenhaut, W., Vass, E., Majer, Z., 2010. Chirality and the origin of atmospheric humic-like substances. Atmos. Chem. Phys. 10, 1315–1327.

Sato, M., Hansen, J., Koch, D., Lacis, A., Ruedy, R., Dubovik, O., Holben, B., Chin, M., Novakov, T., 2003. Global atmospheric black carbon inferred from AERONET. Proc. Natl. Acad. Sci. 100, 6319–6324.

Subramanian, R., Khlystov, A.Y., Robinson, A.L., 2006. Effect of peak inert-mode temperature on elemental carbon measured using thermal-optical analysis. Aerosol Sci. Technol. 40, 763–780.

Tian, J., Chow, J.C., Cao, J., Han, Y., Ni, H., Chen, L., Wang, X., Huang, R., Watson, J.G., 2015. A Biomass Combustion Chamber: Design, Evaluation, and a Case Study of Wheat Straw Combustion Emission Tests. Aerosol Air Qual. Res. 15, 2104–2114.

Wang, Q., Huang, R.-J., Cao, J., Han, Y., Wang, G., Li, G., Wang, Y., Dai, W., Zhang, R., Zhou, Y., 2014. Mixing state of black carbon aerosol in a heavily polluted urban area of China: Implications for light absorption enhancement. Aerosol Sci. Technol. 48, 689–697.

Watson, J.G., 2002. Visibility: science and regulation. J. Air Waste Manag. 52, 628–713.

Watson, J.G., Chow, J.C., Chen, L.-W.A., 2005. Summary of organic and elemental carbon/black carbon analysis methods and intercomparisons. J. Aerosol. Air Qual. Res. 5, 65–102.

Yokelson, R.J., Susott, R., Ward, D.E., Reardon, J., Griffith, D.W.T., 1997. Emissions from smoldering combustion of biomass measured by open-path Fourier transform infrared spectroscopy. J. Geophys. Res. 102, 18865–18877.

Zhan, C., Han, Y., Cao, J., Wei, C., Zhang, J., An, Z., 2013. Validation and application of a thermal-optical reflectance (TOR) method for measuring black carbon in loess sediments. Chemosphere 91, 1462–1470.

Zhang, Q., Streets, D.G., Carmichael, G.R., He, K.B., Huo, H., Kannari, A., Klimont, Z., Park, I.S., Reddy, S., Fu, J.S., Chen, D., Duan, L., Lei, Y., Wang, L.T., Yao, Z.L., 2009. Asian emissions in 2006 for the NASA INTEX-B mission. Atmos. Chem. Phys. 9, 5131–5153.

Zhang, T., Cao, J.-J., Chow, J.C., Shen, Z.-X., Ho, K.-F., Ho, S.S.H., Liu, S.-X., Han, Y.-M., Watson, J.G., Wang, G.-H., Huang, R.-J., 2014. Characterization and seasonal variations of levoglucosan in fine particulate matter in Xi'an, China. J. Air Waste Manag. 64, 1317–1327.

Zhang, Y., Ding, A., Mao, H., Nie, W., Zhou, D., Liu, L., Huang, X., Fu, C., 2016. Impact of synoptic weather patterns and inter-decadal climate variability on air quality in the North China Plain during 1980–2013. Atmos. Environ. 124, 119–128.